

# Minimalist Prion-Inspired Polar Self-Assembling Peptides

Marta Díaz-Caballero,<sup>†</sup> Susanna Navarro,<sup>†</sup> Isabel Fuentes,<sup>‡</sup> Francesc Teixidor,<sup>‡</sup> and Salvador Ventura<sup>\*,†</sup>

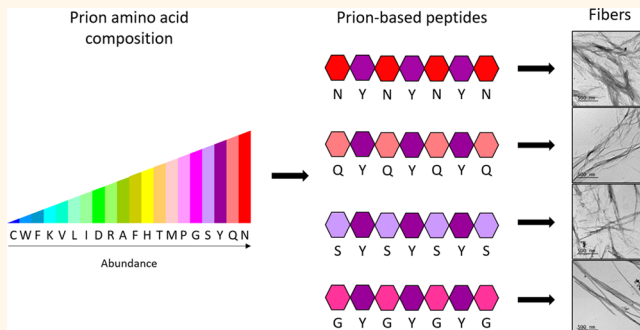
<sup>†</sup>Institut de Biotecnologia i de Biomedicina and Departament de Bioquímica i Biologia Molecular, Universitat Autònoma de Barcelona, 08193 Bellaterra, Barcelona, Spain

<sup>‡</sup>Institut de Ciència de Materials de Barcelona, Campus UAB, 08193 Bellaterra, Barcelona, Spain

## Supporting Information

**ABSTRACT:** Nature provides copious examples of self-assembling supramolecular nanofibers. Among them, amyloid structures have found amazing applications as advanced materials in fields such as biomedicine and nanotechnology. Prions are a singular subset of proteins able to switch between a soluble conformation and an amyloid state. The ability to transit between these two conformations is encoded in the so-called prion domains (PrDs), which are long and disordered regions of low complexity, enriched in polar and uncharged amino acids such as Gln, Asn, Tyr, Ser, and Gly. The polar nature of PrDs results in slow amyloid formation, which allows kinetic control of fiber assembly. This approach has been exploited for fabrication of multifunctional materials because in contrast to most amyloids, PrDs lack hydrophobic stretches that can nucleate their aggregation, their assembly depends on the establishment of a large number of weak interactions along the complete domain. The length and low complexity of PrDs make their chemical synthesis for applied purposes hardly affordable. Here, we designed four minimalist polar binary patterned peptides inspired in PrDs, which include the [Q/N/G/S]-Y-[Q/N/G/S] motif frequently observed in these domains: NYNNYN, QYQQYQ, SYSYSYS, and GYGYG. Despite their small size, they all recapitulate the properties of full-length PrDs, self-assembling into nontoxic amyloids under physiological conditions. Thus, they constitute small building blocks for the construction of tailored prion-inspired nanostructures. We exploited Tyr residues in these peptides to generate highly stable dityrosine cross-linked assemblies for the immobilization of metal nanoparticles in the fibrils surface and to develop an electrocatalytic amyloid scaffold. Moreover, we show that the shorter and more polar NYNNYN, QYQQYQ, and SYSSYS hexapeptides also self-assemble into amyloid-like structures, consistent with the presence of these tandem motifs in human prion-like proteins.

**KEYWORDS:** *self-assembly, amyloid fibrils, prion domain, short peptides, low complexity sequences, nanomaterials.*



Prions are proteins with the amazing capacity to switch between a soluble conformation and a self-perpetuating amyloid state. Initially associated with neurodegenerative diseases,<sup>1</sup> it is now clear that prion-like mechanisms are exploited by different organisms for functional purposes.<sup>2,3</sup> The first functional prions were described in yeast.<sup>4,5</sup> The ability of yeast prions to access an amyloid state is encoded in long, disordered, and low complexity sequences enriched in polar and uncharged amino acids such as Gln, Asn, Tyr, Ser, and Gly, known as prion domains (PrDs).<sup>5</sup> PrDs are both necessary and sufficient for the formation of transmissible amyloid structures.<sup>6</sup> Importantly, sequences displaying this compositional bias seem to be ubiquitous in eukaryotes,<sup>3</sup> and in humans, they account for ~1% of the proteome.<sup>7</sup> Bacteria also exploit prion-like repeats to build up functional amyloids.<sup>8,9</sup>

Amyloid fibrils assemble into highly ordered and extremely stable supramolecular structures.<sup>10</sup> They are useful for a wide range of applications in biotechnology, nanotechnology, and material sciences, since they allow bottom-up manufacturing of materials via self-assembly at room temperature in environmentally benign solvents.<sup>11–13</sup> It has been shown that the PrDs of Ure2 and Sup35 yeast prions, as well as the prion-like domain (PrLD) of the human FUS (Fused in sarcoma) protein, can be used to form functional fibrillar structures for different applied purposes, including the assembly of enzymatically active microgels, biosensors, or metallic nanowires.<sup>14–18</sup> The main

**Received:** January 16, 2018

**Accepted:** May 29, 2018

**Published:** May 29, 2018



advantage of using this kind of domains as self-assembling units is that their intrinsic properties result in slow and tunable assembly kinetics, in such a way that nanofibers can be easily and hierarchically generated across multiple scales.<sup>15</sup> Moreover, the assembly of these, initially disordered domains does not require harsh environments, in contrast to the highly denaturing conditions usually employed to produce amyloid fibrils from globular protein domains.<sup>19,20</sup>

The ability of PrDs to form ordered amyloids is puzzling if one takes into account their polar nature, since it is well-established that the assembly potential of most amyloid proteins is highly dependent on the presence of short sequence stretches with high hydrophobicity.<sup>21,22</sup> Actually, PrDs should fulfill two apparently contradictory properties: remain soluble and disordered during a large part of the protein lifetime and, at the same time, display a cryptic self-assembly propensity that can be triggered under specific conditions.<sup>23</sup> This duality explains the absence of highly amyloidogenic sequences in PrDs,<sup>24</sup> the formation of fibrillary structures relying on the establishment of a large number of weak interactions distributed along the complete low complexity and polar domain sequence.<sup>25,26</sup> The consequence is that PrDs and PrLDs are much larger than the majority of self-assembling peptides used for nanotechnological applications.<sup>11</sup> Traditionally, a minimal length of 80 residues has been suggested to be necessary for the conversion of PrDs into amyloids.<sup>6,24</sup> In this way, Ure2, Sup35, and FUS PrDs consist of 88, 131, and 213 residues, respectively.

The size and low complexity of PrDs make their chemical synthesis difficult and expensive. Here, we explored if much shorter peptides displaying a composition inspired by PrDs, and thus a polar nature, would still have the ability to form ordered assemblies. We show that NYNNYN, QYQQYQYQ, SYSYSYS, and GYGYGYG heptapeptides, as well as NYNNYN, QYQQYQYQ, and SYSSYS hexapeptides, all self-assemble into defined amyloid-like fibrillar structures. We also illustrate how this kind of assembly can be exploited for different nanotechnological purposes.

## RESULTS AND DISCUSSION

**Design of Short Prion-Inspired Self-Assembling Peptides.** The PrLD of FUS, but also of other prion-like human RNA-binding proteins like TAF15, EWSR1, and heterogeneous nuclear (hn)RNPA1 and hnRNPA2 proteins, all able to self-assemble *in vitro* and *in vivo*, have been described to contain imperfect and in some cases overlapping repeats of [G/S]-Y-[G/S].<sup>27–29</sup> The central Tyr in this triplet is essential for self-assembly.<sup>30</sup> Indeed, an analysis of these sequences with the Prosite motif finder (<https://prosite.expasy.org/scanprosite/>) indicates that the motif is best described as [Q/N/G/S]-Y-[Q/N/G/S], and accordingly, it includes the five most enriched residues in PrDs. We decided to exploit this periodicity to design prion-inspired short self-assembling peptides, consisting of overlapping, NYN, QYQ, SYS, or GYG motifs.

Natural amyloid fibrils consist of several protofilaments, each composed of  $\beta$ -strands running perpendicular to the long axis of the fibril, forming a cross- $\beta$  structure. Each filament has typically a diameter of  $\sim 30 \text{ \AA}$ .<sup>31,32</sup> This size includes the  $\beta$ -strands and the turns connecting them. Therefore,  $\beta$ -strands would typically span 20–25  $\text{\AA}$  in the cross- $\beta$  motif.  $\beta$ -Sheets have a translation of 3.2 and 3.4  $\text{\AA}$  per residue in parallel and antiparallel disposition, respectively. Thus, approximately seven

residues can be accommodated in this distance, and accordingly, this length was selected for our sequences. Indeed, the first atomic structure of a short fibril-forming segment of a natural amyloid protein corresponded to the polar seven-residue GNNQQNY stretch of the yeast prion Sup35.<sup>33</sup>

A binary-patterned SYSYSYS heptapeptide would accommodate three overlapping SYS motifs, whereas a YSYSYSY peptide would contain only two. Therefore, the first pattern with four polar and three Tyr residues per hypothetical  $\beta$ -strand was selected. First, we analyzed if the seven-residue-long sequences NYNNYN (NY7), QYQQYQYQ (QY7), SYSYSYS (SY7), and GYGYGYG (GY7) would exhibit any intrinsic propensity to form amyloid assemblies using two well-validated algorithms: PASTA<sup>34</sup> and Tango.<sup>35</sup> Both failed to classify these sequences as amyloidogenic (Table 1), likely because of their

**Table 1. Amino Acid Sequence, Amyloid Propensity Predictions, and Hydropathicity of Designed and  $\text{A}\beta(16\text{--}22)$  Peptides<sup>a</sup>**

peptide	sequence	PASTA	TANGO	Gravy score
NY7	NYNNYN	-1.257939	$5 \times 10^{-16}$	-2.557
QY7	QYQQYQYQ	-1.916377	$8 \times 10^{-21}$	-2.557
SY7	SYSYSYS	-2.090241	$1 \times 10^{-26}$	-1.014
GY7	GYGYGYG	-0.615267	$2 \times 10^{-17}$	-0.786
$\text{A}\beta(16\text{--}22)$	KLVFFAE	-4.53937	1183	1.143

<sup>a</sup>PASTA<sup>34</sup> and TANGO<sup>35</sup> were used to predict the amyloid propensity of the peptides. PASTA sequences with scores less than -4.0 are considered amyloidogenic. Gravy score was calculated with the ProtParam tool integrated in ExPASy,<sup>38</sup> the more positive the score, the more hydrophobic the sequence.

much lower hydropathicity, when compared with that of classical stretches of the same size present in pathogenic amyloidogenic proteins like the  $\text{A}\beta$  peptide (Table 1). However, there is the possibility that, as in the case of PrDs and PrLDs their composition and periodicity would endorse these sequences with a cryptic amyloid propensity that might still allow their self-assembly. We decided to test this possibility experimentally. Indeed, short amphiphilic peptides alternating polar/nonpolar residues have been already shown to self-assemble.<sup>36,37</sup>

**Short Prion-Inspired Peptides Assemble into  $\beta$ -Sheet-Rich Structures.** Heptapeptides NY7, QY7, SY7, and GY7 were synthesized. N-Terminal acetylation and C-Terminal amidation were used to neutralize terminal charges and mimic the protein environment. The lyophilized peptides were resuspended in 1,1,1,3,3-hexafluoropropanol at a final concentration of 10 mM, divided into aliquots, and frozen at  $-80^\circ\text{C}$  until further analysis.

Subtle differences in solution conditions can dramatically influence the pathway of amyloid formation and the detailed morphology of the final fibrillar structures.<sup>39</sup> Therefore, we explored the ability of the peptides to self-assemble in two different pHs (6.0 and 7.0) and two different ionic strengths (without and with 150 mM NaCl). Buffers were named in the following manner: buffer A (100 mM  $\text{KH}_2\text{PO}_4$ , pH 6.0), buffer B (100 mM  $\text{KH}_2\text{PO}_4$ , pH 7.0), buffer C (100 mM  $\text{KH}_2\text{PO}_4$ , pH 6.0 and 150 mM NaCl), and buffer D (100 mM  $\text{KH}_2\text{PO}_4$ , pH 7.0 and 150 mM NaCl).

The results obtained upon incubation of NY7, QY7, SY7, and GY7 in buffer B are shown in Figures 1–4, respectively,

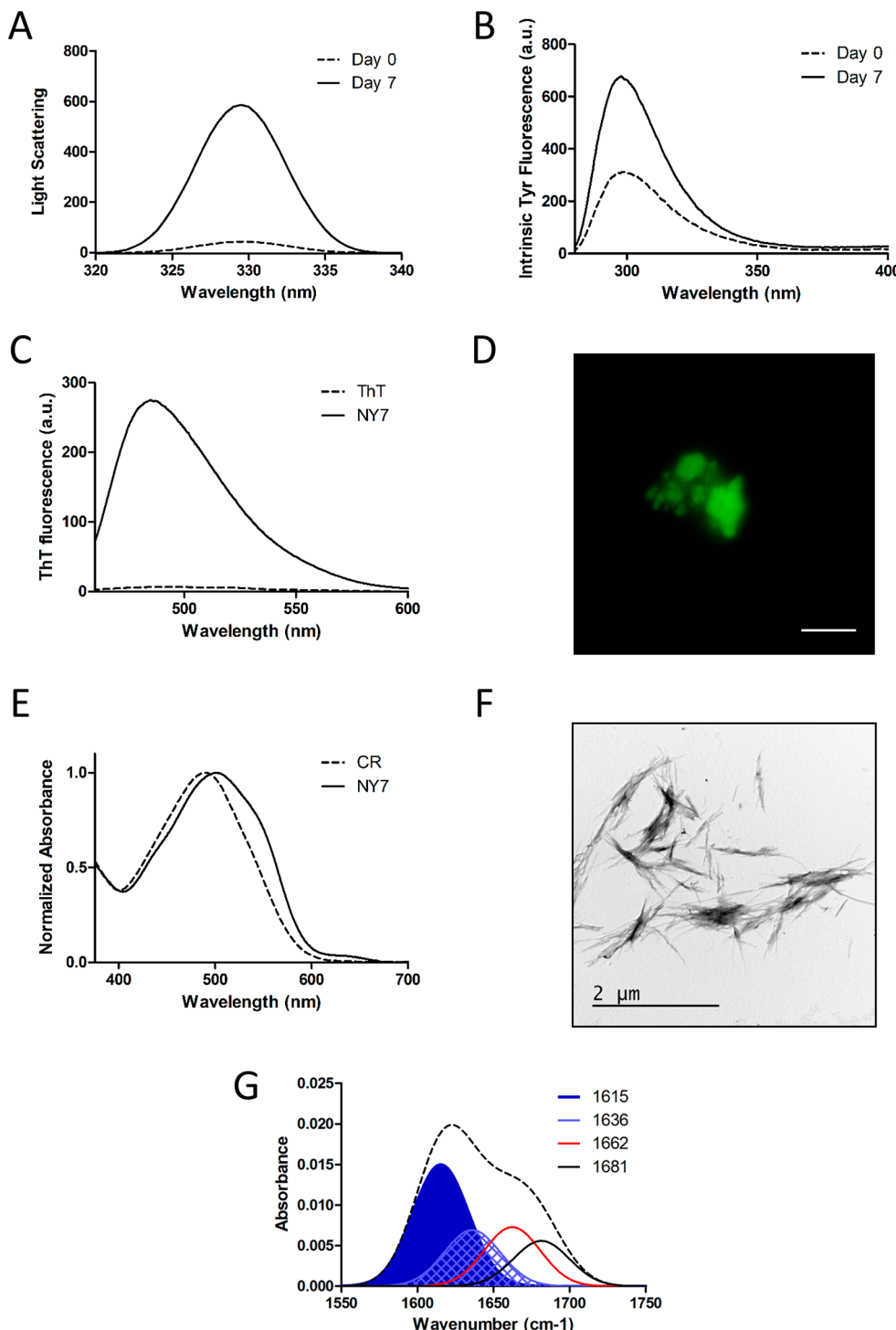


**Figure 1. NY7 peptide biophysical characterization.** NY7 peptide was prepared at 250  $\mu\text{M}$  in buffer B and analyzed at 0 (dashed line) and 7 days (solid line) of incubation: (A) Synchronous light scattering. (B) Intrinsic tyrosine fluorescence. (C) Th-T and (E) CR binding assays in the absence (dashed line) and in the presence (solid line) of NY7. (D) Fluorescence microscopy images of NY7 stained with Th-T. Scale bar corresponds to 20  $\mu\text{m}$ . (F) Representative TEM micrograph. (G) FT-IR absorbance spectrum in the amide I region (dashed line); the blue colored and meshed areas indicate the intermolecular  $\beta$ -sheet signals contribution to the total spectrum area.

whereas the data for the rest of conditions are shown in Figures S1–S4. Peptides NY7, QY7, and SY7 were incubated at 250  $\mu\text{M}$ . Incubation of GY7 at 250  $\mu\text{M}$  resulted in the formation of detectable peptide aggregates, but they did not exhibit evident amyloid signatures under any of the incubation conditions (Figure S5 illustrates the data obtained in buffer B), and

accordingly, a final concentration of 500  $\mu\text{M}$  was used for this peptide in all subsequent experiments.

To investigate the ability of the peptides to self-assemble, we first monitored the evolution of synchronous light scattering signal of incubated peptides. Maximum and stable light scattering signals were obtained upon 7 days incubation at 25 °C. Therefore, all subsequent biophysical parameters were

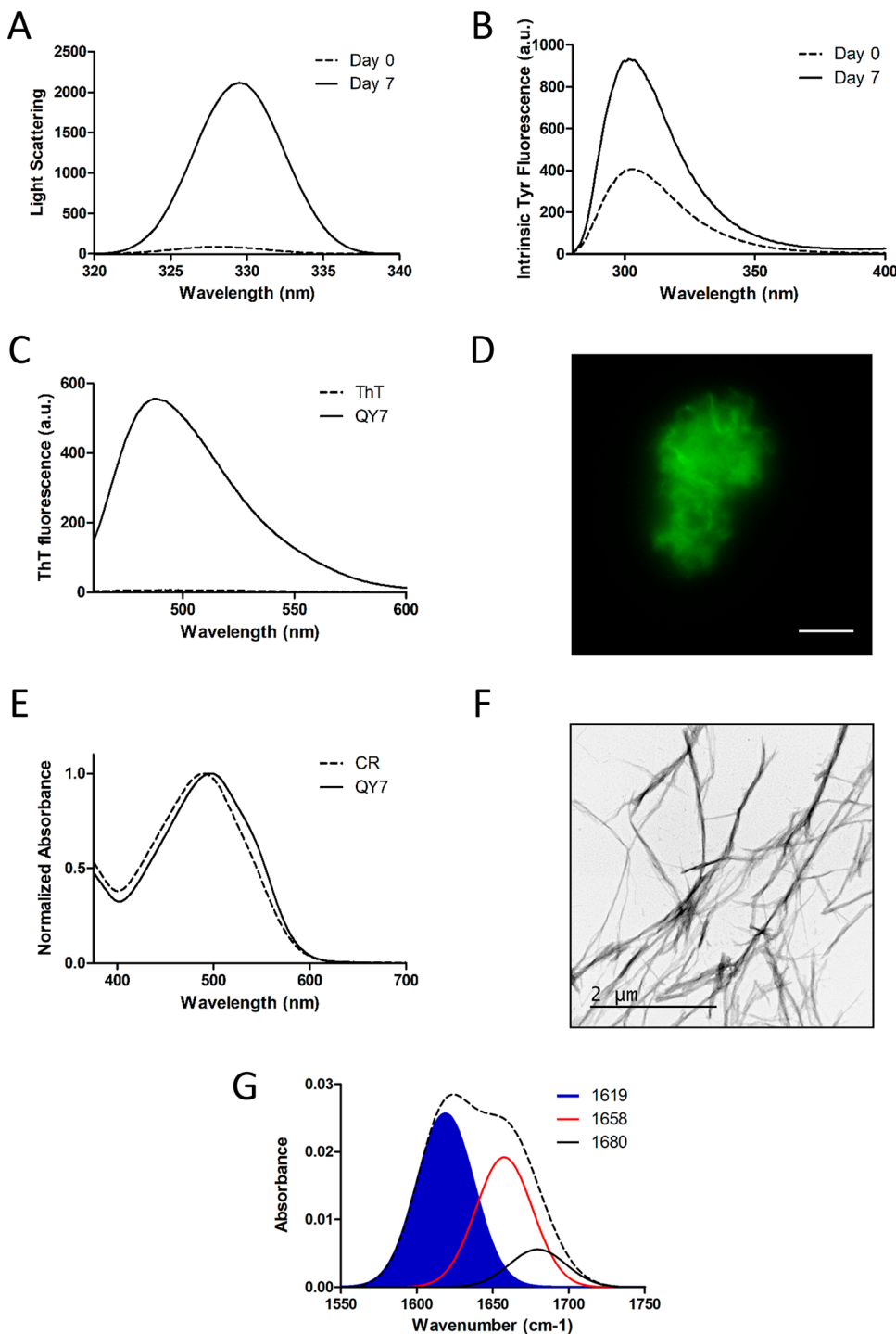


**Figure 2.** QY7 peptide biophysical characterization. QY7 peptide was prepared at 250  $\mu$ M in buffer B and analyzed at 0 (dashed line) and 7 days (solid line) of incubation: (A) Synchronous light scattering. (B) Intrinsic tyrosine fluorescence. (C) Th-T and (E) CR binding assays in the absence (dashed line) and in the presence (solid line) of QY7. (D) Fluorescence microscopy images of QY7 stained with Th-T. Scale bar corresponds to 20  $\mu$ m. (F) Representative TEM micrograph. (G) FT-IR absorbance spectrum in the amide I region (dashed line); the blue colored and meshed areas indicate the intermolecular  $\beta$ -sheet signals contribution to the total spectrum area.

measured at this time point. For the NY7, QY7, and SY7 peptides, a large increase in light scattering signal upon incubation was observed under all conditions (Figures 1A–3A and S1A–S3A), relative to the respective soluble counterparts. For GY7, the increase in light scattering is also significant under all conditions but lower than the rest of peptides (Figures 4A and S4A).

Each designed peptide contains three Tyr residues, with the intrinsic fluorescence of this residue being sensitive to its environment.<sup>40</sup> Hence, we recorded the Tyr fluorescence spectra of soluble and incubated peptides to test whether their assembly produces any detectable structural rearrangement. Upon incubation, the intensity for emission maxima of Tyr increases significantly for the NY7 peptide under all conditions (Figures 1B and S1B). This enhancement is usually attributed

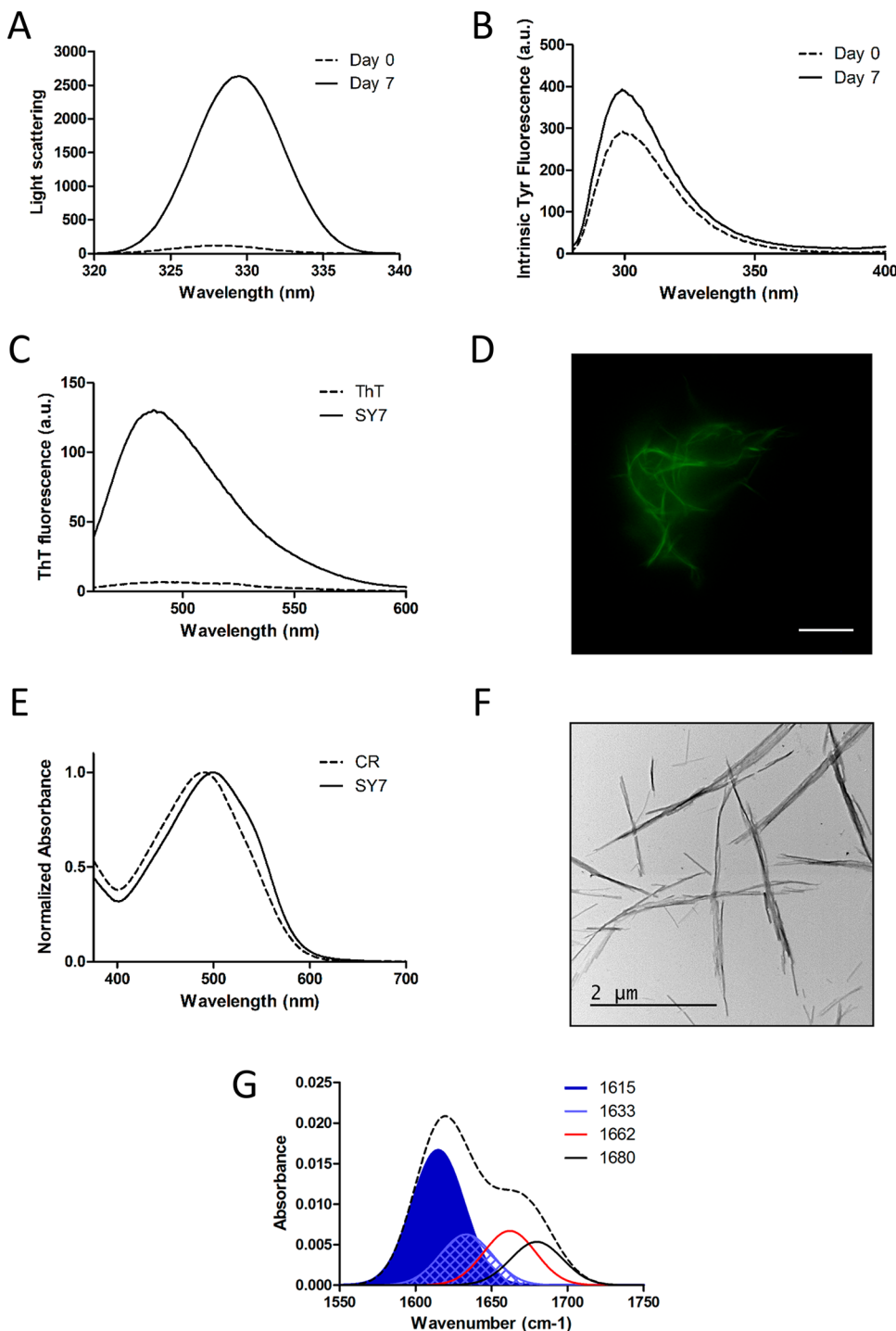


**Figure 3. SY7 peptide biophysical characterization.** SY7 peptide was prepared at 250  $\mu$ M in buffer B and analyzed at 0 (dashed line) and 7 days (solid line) of incubation: (A) Synchronous light scattering. (B) Intrinsic tyrosine fluorescence. (C) Th-T and (E) CR binding assays in the absence (dashed line) and in the presence (solid line) of SY7. (D) Fluorescence microscopy images of SY7 stained with Th-T. Scale bar corresponds to 20  $\mu$ m. (F) Representative TEM micrograph. (G) FT-IR absorbance spectrum in the amide I region (dashed line); the blue colored and meshed areas indicate the intermolecular  $\beta$ -sheet signals contribution to the total spectrum area.

to the change in the local environment of the fluorophore from an initially hydrophilic context, where Tyr residues would be randomly oriented in solution and easily quenched by the solvent, to a more protected environment. The same effect was observed for the QY7 peptide in buffers B–D, whereas the increase in fluorescence was more moderate in buffer A (Figures 2B and S2B). For the SY7 peptide, moderate increases in Tyr fluorescence emission were detected in buffers A and B

but not in the presence of 150 mM NaCl (buffers C and D) (Figures 3B and S3B). With the exception of buffer C, no increase in Tyr fluorescence signal was obvious for the GY7 peptide (Figures 4B and S4B).

Next, we monitored if upon incubation any of the peptides was able to acquire a  $\beta$ -sheet-enriched structure, a common hallmark for amyloid fibril formation. To this aim we used Fourier-transform infrared (FT-IR) spectroscopy and recorded

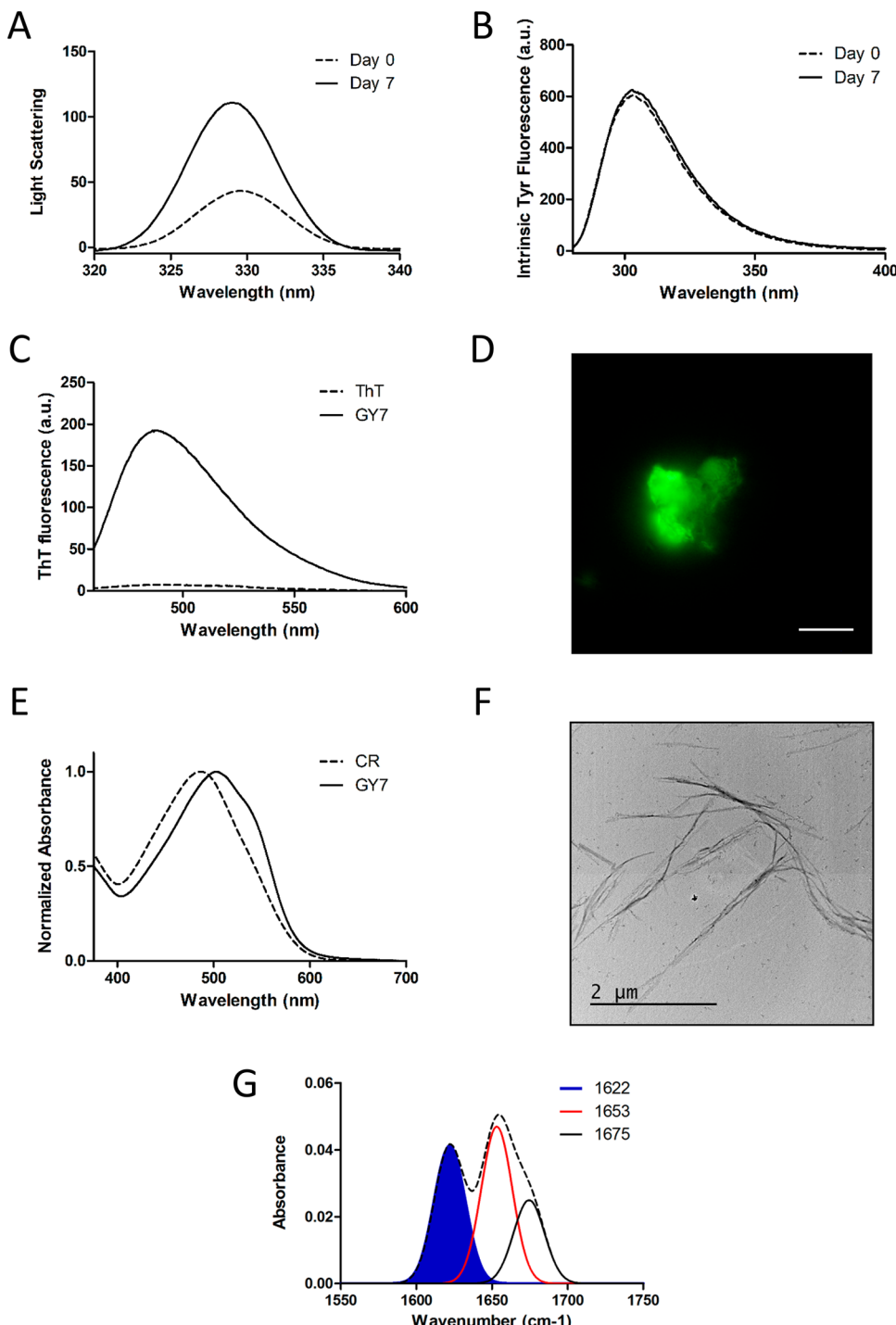


**Figure 4. GY7 peptide biophysical characterization.** GY7 peptide was prepared at 500  $\mu$ M in buffer B and analyzed at 0 (dashed line) and 7 days (solid line) of incubation: (A) Synchronous light scattering. (B) Intrinsic tyrosine fluorescence. (C) Th-T and (E) CR binding assays in the absence (dashed line) and in the presence (solid line) of GY7. (D) Fluorescence microscopy images of GY7 stained with Th-T. Scale bar corresponds to 20  $\mu$ m. (F) Representative TEM micrograph. (G) FT-IR absorbance spectrum in the amide I region (dashed line); the blue colored area indicates the intermolecular  $\beta$ -sheet signal contribution to the total spectrum area.

the amide I region of the spectrum ( $1700\text{--}1600\text{ cm}^{-1}$ ) (Figures 1G–4G and Table S1). For these assays we selected buffer B, where on the average the increase in light scattering was higher for the conjunct of peptides. The amide I spectral region corresponds to the absorption of the carbonyl peptide bond group of the protein main chain and is sensitive to the peptide conformation. Deconvolution of the spectra allowed us to assign the secondary structure elements and their relative

contribution to the main absorbance (Table S1). The spectra of all incubated peptides display signals indicative of the formation of  $\beta$ -sheet structure, coming both from the intermolecular  $\beta$ -sheet region at  $1615\text{--}1636\text{ cm}^{-1}$  and the  $\beta$ -turn region comprised between  $1675$  and  $1682\text{ cm}^{-1}$ , which together account for >50% of the spectral area in all the cases. Interestingly, no antiparallel  $\beta$ -sheet band was detected ( $\sim 1690\text{ cm}^{-1}$ ) in any of the samples, thus suggesting that the detected

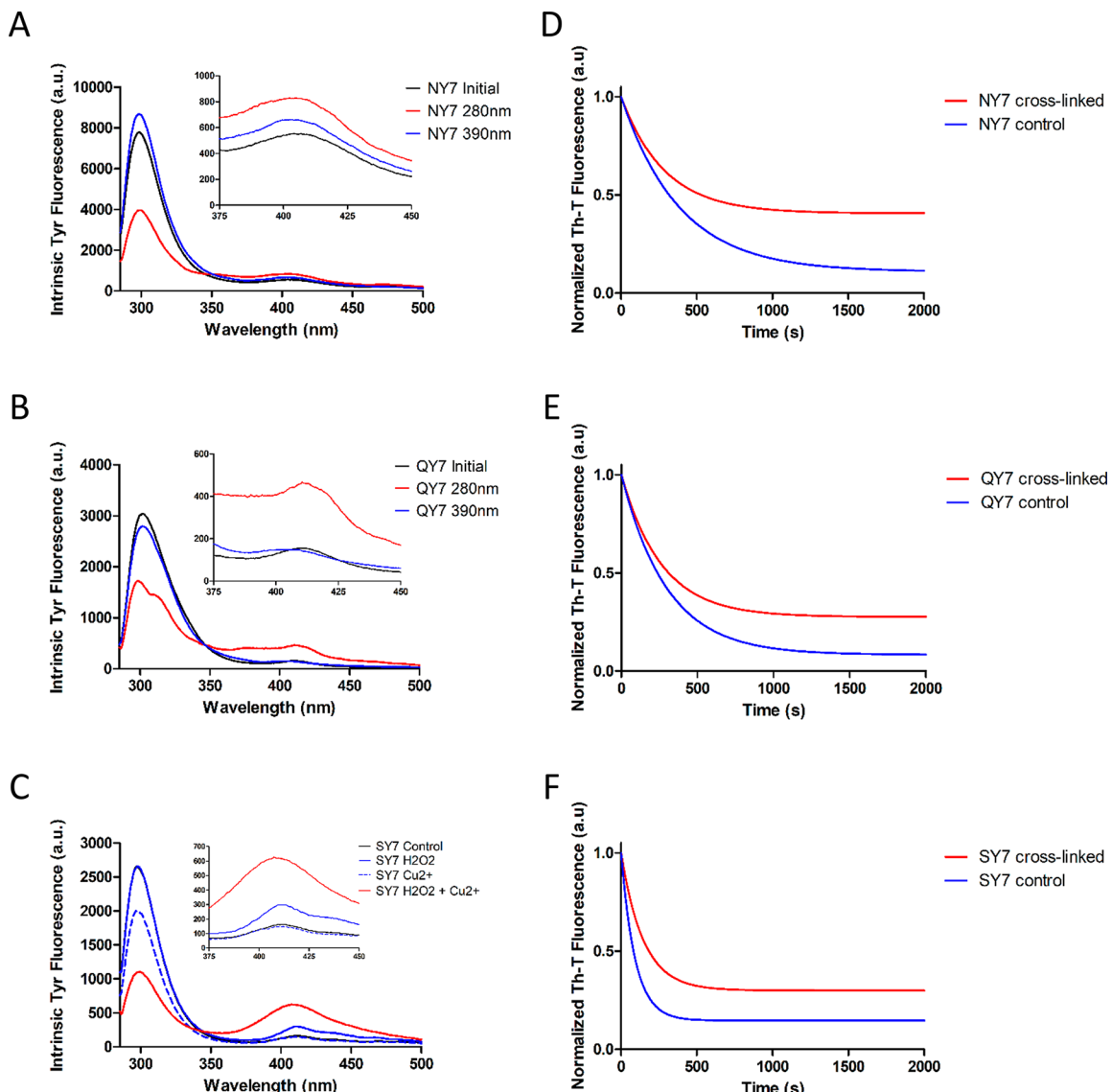


**Figure 5.** NY7, QY7, and SY7 fibrils dityrosine cross-link and denaturation. NY7, QY7, and SY7 fibrils were assembled at 250  $\mu$ M. NY7 and QY7 fibrils were cross-linked using UV-light. Measurements were performed before (black line) and after (red line) irradiation at 280 nm; a control was irradiated at 390 nm (blue line). (A and B) Fibrils spectra upon excitation at 274 nm. Insets show the dityrosine emission region (375–450 nm). SY7 peptide fibrils were chemically cross-linked. Measurements were performed with without treatment (black line), upon incubation with  $\text{Cu}^{2+}$  and  $\text{H}_2\text{O}_2$  (red line), upon incubation with  $\text{Cu}^{2+}$  only (dashed blue line) and upon incubation with  $\text{H}_2\text{O}_2$  only (solid blue line). (C) Fibrils spectra upon excitation at 274 nm. Insets show the dityrosine emission region (375–450 nm). (D–F) Chemical denaturation was performed with 2 M GITC in the case of NY7 (D) and SY7 (F) and with 3 M GITC for QY7 (E), followed by monitoring the Th-T signal.

$\beta$ -strands in the self-assembled peptides might adopt a preferentially parallel disposition. The other detected signals were associated with the presence of disordered structure and turns and contributed  $\sim 20\%$  of the signal in the case of peptides NY7 and SY7 and  $\sim 40\%$  for peptides QY7 and GY7.

**Short Prion-Inspired Peptides Assemble into Amyloid-like Fibrillar Structures.** To assess if the identified  $\beta$ -sheet-containing assemblies might correspond to amyloid-like structures, we used amyloid-specific dyes Thioflavin-T (Th-T) and Congo Red (CR). Th-T is an amyloid-binding dye which fluorescence emission maximum at 488 nm increases in the presence of amyloid-like structures.<sup>41</sup> To detect the presence of amyloid conformations, Th-T fluorescence emission spectra were recorded in the presence of the incubated samples (Figures 1C–4C and S1C–S4C). For all peptides and under all

conditions, a large increase in the intensity of Th-T fluorescence emission signal was observed. However, for any particular peptide the increase in Th-T signal depended on the incubation conditions, thus indicating that the interplay between sequence and environment modulates the amount or the conformation of amyloid assemblies in the peptides solutions. In order to confirm the formation of structures able to bind Th-T by the incubated peptides, buffer B was selected, and fluorescence microscopy images of Th-T stained samples were acquired. In all cases, the presence of green-yellow fluorescent structures against a dark background was evidenced (Figures 1D–4D).

To confirm the presence of amyloid assemblies, we also used CR, as second amyloid-specific dye. Addition of CR to the incubated peptides resulted in a clear red-shift of its absorption

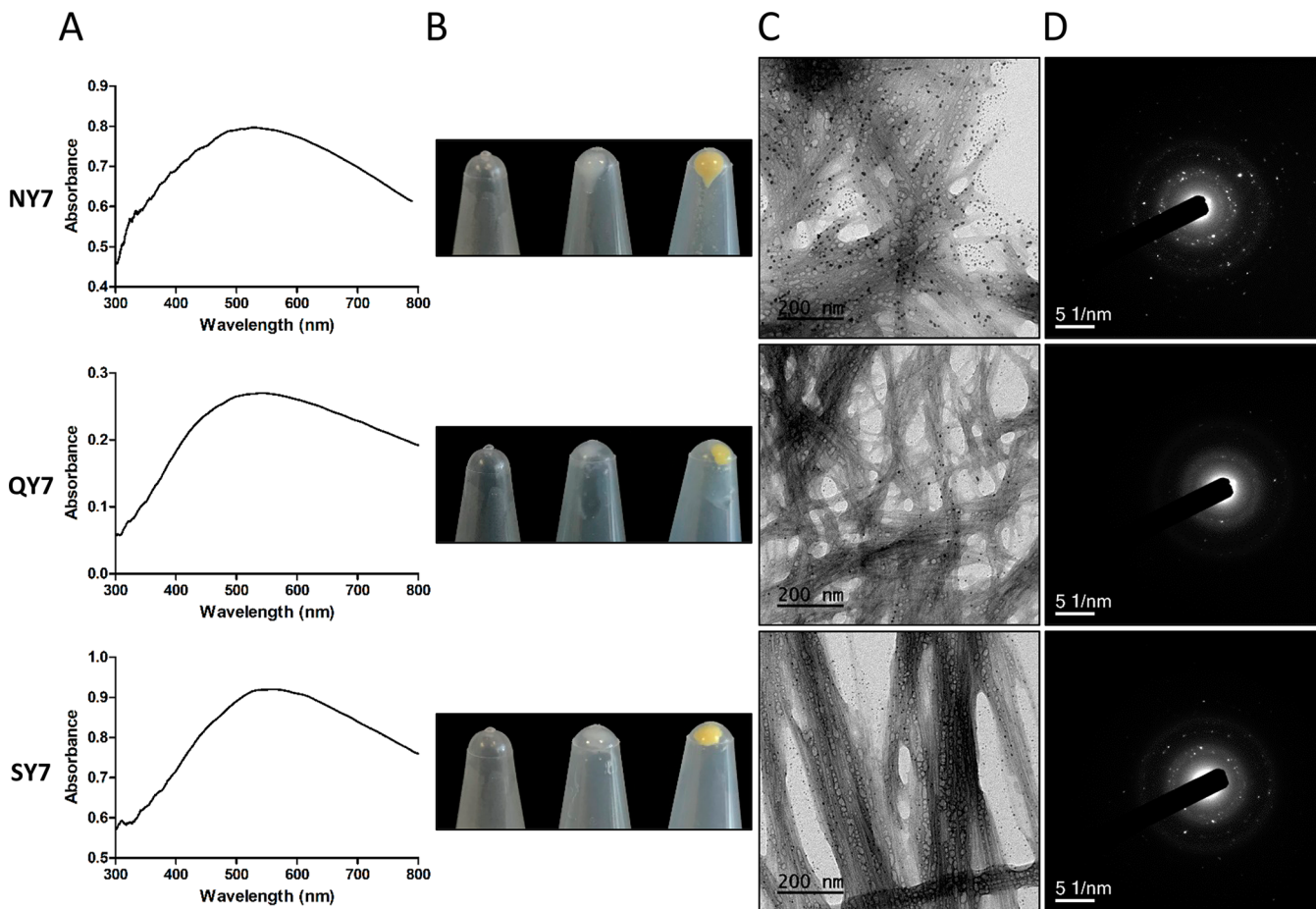


**Figure 6.** Formation of silver nanoparticles on NY7, QY7, and SY7 fibrils. Absorbance spectra of peptide fibrils assembled at 250  $\mu$ M and decorated with silver nanoparticles (AgNP) in buffer B. (B) From left to right: pellets obtained upon incubation of an AgNO<sub>3</sub> solution without fibrils, fibrils without AgNO<sub>3</sub>, and fibrils with AgNO<sub>3</sub> for 24 h. The yellow color corresponds to AgNP. (C) TEM micrographs of fibrils decorated with AgNP. (D) Electronic diffraction pattern from fibrils shown in panel (C).

spectra, indicative of the dye binding to an amyloid structure<sup>42</sup> in all cases except for the NY7 peptide in the presence of 150 mM NaCl (buffers C and D) (Figures 1E–4E and S1E–S4E), consistent with a low binding of this peptide to Th-T under these particular conditions.

Amyloid-like assemblies display a fibrillar macromolecular architecture which can be visualized by negative-staining and transmission electron microscopy (TEM). To explore the morphological features of incubated peptides, they were deposited over copper grids and negatively stained with uranyl acetate. The analysis of representative micrographs of peptides incubated in buffer B confirms the presence of fibrillar assemblies for the NY7, QY7, SY7, and GY7 variants (Figures 1F–4F), all displaying long, thin, and regular amyloid fibers. Measurements of length and thickness using high-magnification micrographs (Figure S6) indicated that they are 18–25 nm wide and with lengths ranging from 0.5 to 5  $\mu$ m (Table S2), thus having dimensions similar to those of canonical amyloid fibrils.<sup>43</sup>

**Short Prion-Inspired Peptides Amyloid Assemblies Are Nontoxic.** A main limitation for the use of amyloid fibrils for applied biomedical purposes comes from the fact that these assemblies might possess cytotoxic activity. In order to test whether the observed amyloid-like fibrils were neurotoxic, the incubated peptides were added to cultured neuroblastoma SH-SY5Y cells at concentrations ranging from 5 to 50  $\mu$ M. After 72

h of incubation, cytotoxicity was assessed. None of the peptides exerted a toxic effect on neuronal cultures at any of the tested concentrations (Figure S7).

**Tyrosine Cross-Linking Renders Highly Resistant Prion-Inspired Amyloid Assemblies.** Tyrosine cross-links stabilize numerous natural biopolymer systems,<sup>44</sup> and they have been exploited to increase the strength of synthetic peptide-based nanostructures.<sup>45</sup> Because each of our peptides contains three Tyr, we explored whether amyloid fibrils could be covalently cross-linked through the formation of dityrosines (DiY) and, in this case, if the reaction results in more stable assemblies. For these experiments, we selected the NY7, QY7, and SY7 variants because their self-assembly occurs at lower peptide concentrations and results in the formation of microscopic fibrillar meshes, as imaged by TEM (Figure S8).

First, the fibrils formed by NY7, QY7, and SY7 peptides were UV-irradiated to generate DiY-modified assemblies. UV-irradiation-induced Tyr cross-linking can be monitored by fluorescence spectroscopy. In our peptides, Tyr constitutes the only target for photooxidative modifications. We applied UV irradiation at 280 nm to selectively excite Tyr and convert it into a radical, which should lead to the formation of DiY, its major photooxidation product. An equal aliquot of fibrils was irradiated at 390 nm, outside of the Tyr excitation spectrum, as a control. As shown in Figure 5A,B, excitation of NY7 and QY7 fibrils at 280 nm for 25 min leads to a significant decrease in the

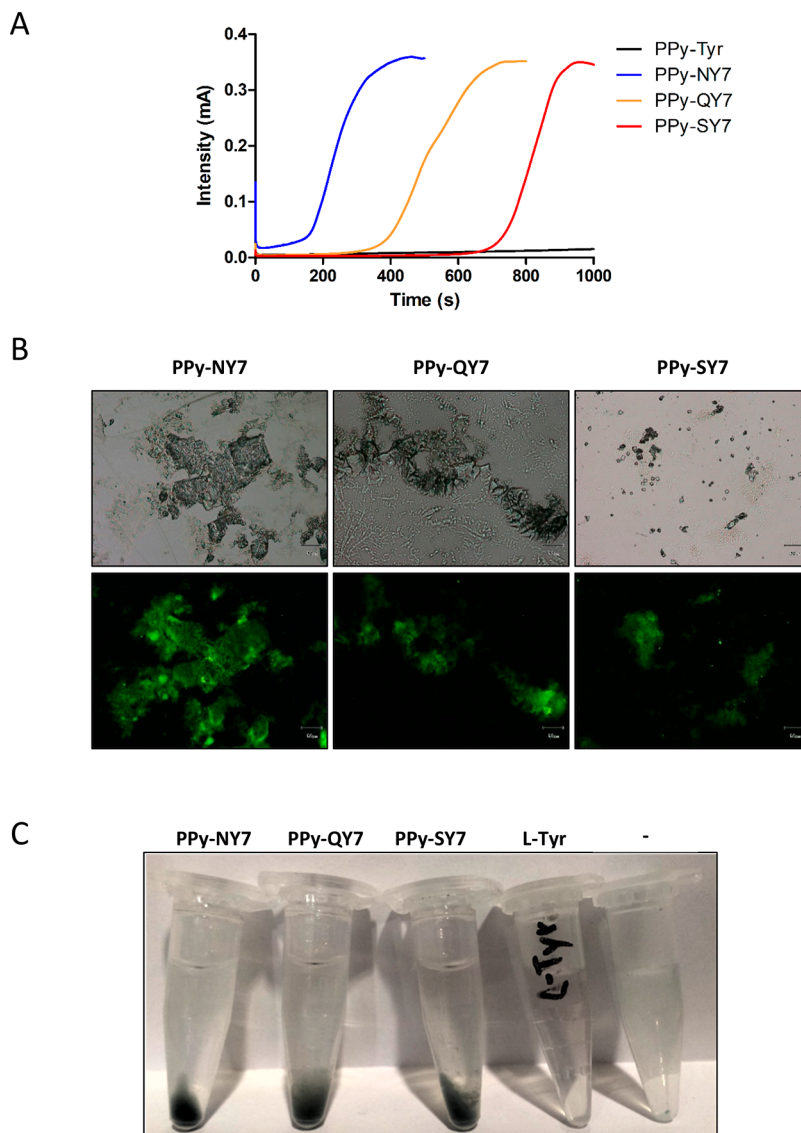


**Figure 7.** NY7, QY7, and SY7 fibrils act as bioelectrocatalysts. (A) Chronoamperometry curve of the electropolymerization of pyrrole into polypyrrole (PPy) using peptides NY7 (red), QY7 (green), SY7 (blue), and L-tyrosine monomer (black). Potential applied at 0.7 V vs Ag/AgCl in 0.1 M NaCl containing 50 mM pyrrole and 250  $\mu$ M peptide fibrils. (B) Optical microscope images of PPy-peptides with and without fluorescence. From left to right, PPy-NY7, PPy-QY7, and PPy-SY7. Scale bar corresponds to 30  $\mu$ m. (C) Image taken 24 h after the chemical polymerization with distillate pyrrole vapor. Solutions contained CuCl<sub>2</sub> and the indicated peptide or L-Tyr or CuCl<sub>2</sub> only (−). The solutions were centrifuged for 5 min at 6000g.

Tyr intrinsic fluorescence signal (305 nm), concomitant with an increase in fluorescence emission intensity at 405–410 nm, indicating DiY formation. This was confirmed exciting the fibrils at the DiY excitation maximum (320 nm) and recording the fluorescence emission of DiY in the 350–475 nm range (Figure S9A,B). Next, we monitored the kinetics of DiY formation irradiating at 280 nm and recording the fluorescence emission at 410 nm. In Figure S9C,D it is shown how for both NY7 and QY7 the DiY signal increased with UV-irradiation time, whereas irradiation at 390 nm did not have any effect. We used TEM to confirm that the UV-irradiated samples display an amyloid-like morphology (Figure S9E,F).

The impact of UV-irradiation on fibril Tyr cross-linking was also evident for SY7 but weaker than for NY7 and QY7 (Figure S10). Therefore, for this peptide we used chemical induced DiY formation. As shown in Figures 5C and S9G, incubation of SY7 fibrils with Cu<sup>2+</sup> and H<sub>2</sub>O<sub>2</sub> for 24 h induces DiY formation,

whereas incubation in buffer alone, buffer supplemented only with Cu<sup>2+</sup>, or only with H<sub>2</sub>O<sub>2</sub> has a minor effect. We confirmed by TEM that Cu<sup>2+</sup> + H<sub>2</sub>O<sub>2</sub> treatment allows maintenance of a fibrillar morphology (Figure S9H).

Next, we assessed if the introduced covalent linkages resulted in a stronger assembly. To this aim, we evaluated the fibril's stability against chemical denaturation. It turned out that nontreated fibrils were already significantly resistant to urea and guanidinium hydrochloride (GuHCl) (Figure S11); thus, we used the stronger denaturing agent guanidinium isothiocyanate (GITC) for the experiments. For the three peptide variants, the amyloid structure is lost more slowly and to a lower extent upon incubation in GITC for DiY-cross-linked fibrils than for nontreated samples, as evidenced by recording the changes in Th-T fluorescence signal with time (Figure S5D–F). This confirms that the introduced cross-links significantly stabilize the amyloid structure.

### Metallization of Prion-Inspired Amyloid Assemblies.

The capability of Tyr to facilitate bioreduction without the need of a chemical reducing agent or additives has been exploited for the mineralization of peptide assemblies.<sup>46</sup> Tyr has been shown to reduce silver ions to elemental silver at physiological pH through proton-coupled electron transfer.<sup>47</sup> We assayed if the Tyr residues in NY7, QY7, and SY7 peptides allowed the decoration of fibrils with silver nanoparticles (AgNP), since this kind of biomineratization might find application in molecular electronics. Fibrils were mixed with 3 mM aqueous silver nitrate and incubated for 24 h. A silver nitrate solution without fibrils and a fibril solution without silver nitrate were incubated under the same conditions. Only in the presence of fibrils and silver nitrate did the solution turn yellow, indicating that silver ions were reduced to AgNP, exhibiting the characteristic plasmon absorption band at ~500 nm (Figure 6A). Centrifugation of the solutions evidenced that AgNP were attached to the fibrillar material, since the pellet exhibited the characteristic yellow color (Figure 6B). To confirm this extent, fibrils were mixed with 1 mM aqueous silver nitrate for 24 h, centrifuged, resuspended in 100 mM phosphate at pH 7.0, and imaged without any further staining by TEM. The presence of individual electrodense AgNP located preferentially on the surface of the three peptide fibrils was observed (Figure 6C). Moreover, electron diffraction of the same samples rendered, in the three cases, a diffraction pattern (Figure 6D) that could be univocally assigned to metallic silver (Table S3). Overall, the data indicate that once reduced by Tyr residues the silver metal remains bound to the fibrils likely thanks to the intrinsic affinity of the metal for Tyr<sup>48</sup> resulting in the formation of an AgNP decorated fibrillar surface.

**Prion-Inspired Amyloid Assemblies Act As Bioelectrocatalytic Scaffolds.** One potential application of Tyr-containing peptide assemblies is their use as a redox-active scaffold to develop an enzyme mimetic catalyst.<sup>49</sup> Monomeric tyrosyl radicals are easily quenched in aqueous solution. However, the chemical environment in prion-inspired amyloid assemblies might endorse their Tyr radicals with reduction potentials high enough to catalyze chemical reactions. In particular, we explored whether NY7, QY7, and SY7 fibrils might act as bioelectrocatalysts of pyrrole polymerization.

Polymerized (PPy) can be synthesized electrochemically by applying a potential greater than 0.8 V vs Ag/AgCl or chemically by using an oxidant agent. Although electropolymerization can be initiated at ~0.7 V vs Ag/AgCl, the rate at this potential is too slow to attain macroscopic polypyrrrole deposition.<sup>50</sup> Our results showed that at 0.7 V vs Ag/AgCl a negligible amount of polypyrrrole was produced using the monomer L-Tyrosine (15 μA at 1000 s) (Figure 7A). In contrast, when this voltage was applied to NY7, QY7, and SY7 fibrils, a black macroscopic PPy was deposited continuously (350 μA) (Figure 7A). The intrinsic fluorescence of Tyr residues was exploited to demonstrate that fibrils and polypyrrrole deposits colocalize (Figure 7B). The chronoamperometry curves show how depending on the fibril variant the maximum of pyrrole electropolymerization takes place at different times, in particular at 450, 750, and 950 s for NY7, QY7, and SY7, respectively, not only indicating that in all three cases the peptide performs as an electrocatalyst but also suggesting that the electrocatalytic activity is different for each peptide (Figure 7A). The different times of electrodeposition might be related to the different nature of the non-Tyr residues,

opening an avenue to shape the bioelectrocatalytic properties of Tyr-containing peptide assemblies by tuning their sequences.

We explored whether our prion-inspired amyloid fibrils would allow Cu(II) ions to oxidize pyrrole and thus promote PPy formation through tyrosyl mediated electron transfer, without applying any additional potential. The electrocatalytic activity of NY7, QY7 and SY7 fibrils was assayed by dissolving them in a 4 mM CuCl<sub>2</sub> solution. Solutions containing monomeric Tyr and CuCl<sub>2</sub> or CuCl<sub>2</sub> only were used as controls. The solutions were exposed to pyrrole vapor (Figure S12A). In agreement with the electrochemical studies, after incubation for 24 h, only the peptide containing tubes exhibited a black material, corresponding to PPy that precipitated together with amyloid fibrils (Figure 7C). The deposition of PPy on top of fibrils allowed them to be observed by TEM without any additional staining (Figure S12B). Overall, the data indicate that the chemical environment of Tyr in prion-inspired amyloid fibrils allow them to act as biocatalytic scaffolds.

### Prion-Inspired Hexapeptides Assemble into Amyloid

**Fibrils.** Despite overlapping [Q/N/G/S]-Y-[Q/N/G/S] motifs existing in natural PrDs and PrLDs, accounting for <15% of the repeats, the [Q/N/G/S]-Y-[Q/N/G/S] triplets are more often separated by spacers or adjacent to each other, without the presence of a central Tyr, likely because a binary pattern of Tyr like the one designed in our peptides might lead to uncontrolled self-assembly *in vivo*.

Luo and co-workers have just shown that two hexapeptides correspondent to the PrLD of FUS protein, SYSSYG and SYSGYS, form amyloid fibrils when assembled at 4 °C.<sup>51</sup> We tested whether NYNNYN (NY6), QYQQYQ (QY6), and SYSSYS (SY6) hexapeptides would also spontaneously assemble into amyloid-like structures under the same solution conditions and at same temperature than the binary patterned heptapeptides. These peptides are not only smaller but also more polar than the correspondent heptapeptides. Still, as shown in Figures S13–S15, when dissolved at 500 μM in buffer B and at 25 °C for 7 days, all them formed assemblies that bound to Th-T and CR, displaying a characteristic amyloid morphology when imaged by TEM. It is worth noting here that our peptides assembled at a concentration (~0.4 mg/mL) 50 times lower than the one used by Luo and co-workers in their study (20 mg/mL).<sup>51</sup> The data indicates that the central Tyr is dispensable to attain an amyloid assembly; however, these fibrils were less resistant in front of chemical denaturation than the ones formed by NY7, QY7, and SY7 (Figure S16).

## CONCLUSIONS

Many of the amyloid fibrils used for biotechnological purposes are derived from naturally occurring proteins or peptides known to self-assemble under specific conditions. There is a rising interest in the use of the disordered and low complexity domains characteristic of prion-like proteins to build up multifunctional supramolecular fibrous networks taking profit of their slow assembly kinetics under mild conditions.<sup>14–18</sup> Both the ability to self-assemble and to do it slowly depend on the biased composition of PrDs and PrLDs.<sup>23</sup> We show here that short polar peptides displaying a strict binary pattern of the five more overrepresented amino acids in these domains polymerize into amyloid-like fibrillar structures, as evidenced by FT-IR, Th-T and CR binding, and TEM imaging at different pHs and ionic strengths at low concentrations (<0.3 mg/mL for NY7, QY7, and SY7; <0.4 mg/mL for GY7).

The peptides recapitulate the [Q/N/G/S]-Y-[Q/N/G/S] motif that is recurrently found in the PrLDs of human RNA binding proteins.<sup>27,28</sup> *In vitro*, at concentrations comparable to those found in cells, PrLDs undergo liquid–liquid phase separation.<sup>30,52,53</sup> Over time, or at higher concentrations they can transition into a reversible solid-phase hydrogel.<sup>30,54,55</sup> Such hydrogels are composed of protein fibrils displaying and amyloid-like cross- $\beta$  pattern.<sup>30,56</sup> These fibrils are more labile than those formed by pathogenic proteins, since they lack strongly amyloidogenic hydrophobic sequences. We confirm here that indeed classical amyloid stretches are not necessary for amyloid assembly in PrDs since short [Q/N/G/S]-Y-[Q/N/G/S] segments contain a cryptic but significant amyloid propensity that suffices to drive fibril formation, at least *in vitro*.

What is common to all the heptapeptides in the present study is the presence of three Tyr residues. It is likely that as reported for other short peptides Tyr side chains would contribute to both inter- and intrasheet stabilization.<sup>57</sup> Indeed, aromatic  $\pi$ – $\pi$  interactions play a significant role in the molecular recognition and self-assembly processes of different amyloid proteins,<sup>58</sup> and they have been successfully exploited to build up minimal self-assembling blocks.<sup>59</sup> Together with Tyr, it is expected that Gln, Asn, and Ser would contribute to the adhesive force through hydrogen bonding.<sup>33</sup> Indeed, the recent high-resolution structure of the 168-QYNNQNNFV-176 fragment of the mammalian prion protein in its amyloid state indicates that apart from establishing intermolecular contacts neighboring polar ladders might be additionally linked by hydrogen bonds within strands with adjacent aromatic residues embracing and shielding them thus stabilizing the overall amyloid structure.<sup>60</sup> In contrast to the rest of residues, Gly cannot establish hydrogen bonds, yet GY7 assemblies display all the characteristics of an amyloid. A possible explanation is that similar to what occurs in natural fibrillary proteins<sup>61,62</sup> the small size of this residue allows a close approach of the backbones maximizing van der Waals interactions between adjacent sheets especially if they are not in a fully extended conformation as FT-IR data suggest.

It is clear that the interactions formed by prion-inspired peptides would be weaker than those in the cores of pathogenic fibrils, the assembly of which is rapidly nucleated by multiple intramolecular and intermolecular hydrophobic contacts.<sup>63,64</sup> In fact, the recent resolution of the structures of two tandem [S/G]-Y-[S/G] motifs of the human prion-like protein FUS in their fibrillar forms indicates that the inner architecture of these assemblies differs from the extended  $\beta$ -strand typical of amyloids, resulting in weaker fibrillar structures.<sup>51</sup> This might be also the case for the NY6, QY6, and SY6 peptides in our study, all consisting of a tandem [Q/N/S]-Y-[Q/N/S] motif. Indeed, although they all assemble into ordered amyloid-like structures, these assemblies are weaker than the ones formed by the correspondent heptapeptides.

Overall, we describe here small, nontoxic building blocks to assemble nanofibrillar structures under mild conditions, exploiting prion-inspired intermolecular interactions. We show that as in their much larger PrDs and PrLDs counterparts<sup>14–18</sup> these peptides can be used for different applied purposes. In particular, mimicking the roles played by Tyr groups in enzymes, photoactive proteins, and protein cross-linking, we demonstrate that NY7, QY7, and SY7 peptides can be exploited to attain highly stable materials through DiY formation, to build up fibrils decorated with nanometallic particles, and to be used as scaffolds to catalyze chemical/

electrochemical reactions. Thus, prion-inspired amyloid assemblies appear as promising structures for a number of nanotechnological applications.

## MATERIALS AND METHODS

**Peptides Prediction.** Aggregation propensity of designed peptides was analyzed with two different algorithms: PASTA<sup>34</sup> and TANGO.<sup>35</sup> For all of them, default parameters were used. The Gravy Score, from ProtParam tool in ExPASy,<sup>38</sup> was calculated as indicative of hydrophobicity level of designed peptides.

**Peptides Preparation.** Synthetic peptides NY7 (Ac-NYNYNYNH<sub>2</sub>), QY7 (Ac-QYQYQYQ-NH<sub>2</sub>), SY7 (Ac-SYSYSYS-NH<sub>2</sub>), GY7 (Ac-GYGYGYG-NH<sub>2</sub>), NY6 (Ac-NYNNYN-NH<sub>2</sub>), QY6 (Ac-QYQ-YQ-Q-NH<sub>2</sub>), and SY6 (Ac-SYSSYS-NH<sub>2</sub>) were purchased from CASLO ApS (Scion Denmark Technical University). Lyophilized peptides were dissolved in 1,1,1,3,3,3-hexafluoro-2-propanol to obtain a 10 mM stock solution, divided into aliquots, and frozen at –80 °C.

**Preparation of NY7, QY7, SY7, and GY7 Fibrils.** Peptides were diluted from 10 mM stock to a final concentration of 250  $\mu$ M in 4 different buffers: 100 mM potassium phosphate, pH 6.0 (buffer A); 100 mM potassium phosphate, pH 7.0 (buffer B); 100 mM potassium phosphate, 150 mM NaCl, pH 6.0 (buffer C); and 100 mM potassium phosphate, 150 mM NaCl, pH 7.0 (buffer D). GY7 peptide was also diluted to a final concentration of 500  $\mu$ M in the previously mentioned buffers. For the aggregation reactions, peptides were incubated under quiescent conditions for 7 days at room temperature.

**Preparation of NY6, QY6, and SY6 Fibrils.** Peptides were diluted from 10 mM stock to a final concentration of 500  $\mu$ M in buffer B (100 mM potassium phosphate at pH 7.0). For the aggregation reactions, peptides were incubated under quiescent conditions for 7 days at 25 °C.

**Amyloid Dyes Binding.** Thioflavin T (Th-T) and Congo Red (CR) dyes were used to determine amyloid fibers formation. For Th-T binding assay, incubated peptides were diluted 1:10 in buffer B, and Th-T was added to a final concentration of 25  $\mu$ M. Th-T emission fluorescence was detected on a Jasco FP-8200 fluorescence spectrophotometer (Jasco Corporation, Japan) in the range 460–600 nm, using an excitation wavelength of 445 nm and with an excitation and emission bandwidth of 5 nm. For CR binding assay, incubated peptides were diluted 1:10 in buffer B, and CR was added to a final concentration of 10  $\mu$ M. Optical absorption spectra were recorded from 375 to 700 nm in a Specord200 Plus spectrophotometer (Analytik Jena, Germany). Spectra of protein alone were acquired to subtract protein scattering.

**Light Scattering.** Light scattering was measured in a Jasco FP-8200 fluorescence spectrophotometer (Jasco Corporation, Japan), exciting at 330 nm, and recording in the range 320–340 nm using an excitation and emission bandwidth of 5 nm.

**Tyrosine Intrinsic Fluorescence.** Tyrosine fluorescence spectra was acquired on a Jasco FP-8200 fluorescence spectrophotometer (Jasco Corporation, Japan) in the range 280–400 nm, exciting at 268 nm wavelength, and using an excitation and emission bandwidth of 5 nm.

**Transmission Electron Microscopy (TEM).** For TEM samples preparation, 10  $\mu$ L of the aged fibril solution was deposited onto a carbon-coated copper grid for 10 min, and the excess liquid was removed with filter paper. Uranyl acetate (2% w/v) solution was added for negative staining. Grids were exhaustively scanned using a JEM 1400 transmission electron microscope (JEOL Ltd, Japan) operating at 80 kV, and images were acquired with a CCD GATAN ES1000W Erlangshen camera (Gatan Inc., United States).

**Epifluorescence Microscopy.** Peptides incubated for 7 days were mixed 1:1 with 40  $\mu$ M Th-T in buffer B, and 10  $\mu$ L of the solution was put over a glass slide and covered with a coverslip. Images were obtained on a Nikon Eclipse 90i optic epifluorescence microscope (Nikon, Japan), equipped with a Plan Apo 60 $\times$ /1.4 objective, using the FITC filter. Images were acquired with a Nikon DXM1200F camera (Nikon, Japan).

**Fourier Transform Infrared Spectroscopy.** Assembled fibers were centrifuged at maximum speed 12 000g for 30 min and resuspended in water. Samples were placed on the ATR crystal and dried out. The experiments were carried out in a Bruker Tensor 27 FTIR (Bruker Optics, United States) supplied with a Specac Golden Gate MKII ATR accessory. Each spectrum consists of 32 acquisitions measured at a resolution of 1 cm<sup>-1</sup>. Data were acquired and normalized using the OPUS MIR Tensor 27 software (Bruker Optics, United States). IR spectra were fitted employing a nonlinear peak-fitting equation using PeakFit package v4.12 (Systat Software, San Jose, CA). The area for each Gaussian curve was calculated in the amide I region from 1700 to 1600 cm<sup>-1</sup> using second derivative deconvolution method in PeakFit package v4.12 (Systat Software, San Jose, CA).

**Cell Viability Assay.** Human SH-SY5Y cells were plated into 96-well plates at a density of 4000 cells/well (100 μL/well) in F-12 medium supplemented with 10% FBS and maintained at 37 °C and 5% CO<sub>2</sub> atmosphere. Cells were incubated in the presence of 5, 10, 25, and 50 μM NY7, QY7, SY7, and GY7 fibers for 72 h in triplicates. For controls, the same volume of buffer (100 mM phosphate, pH 7.0) was added. Treated cells were incubated with 10 μL of PrestoBlue Cell Viability Reagent (Invitrogen) for 30 min. Cell viability was determined recording fluorescence at 615 nm, with an excitation wavelength of 531 nm in a Victor3 fluorescent plate reader (PerkinElmer).

**Silver Nanoparticles Conjugation to Peptide Fibrils.** NY7, QY7, and SY7 were assembled as described, were centrifuged at 12 000g for 30 min. Pelleted fibrils were resuspended in the same volume of 1 or 3 mM AgNO<sub>3</sub> in water and incubated for 24 h at 25 °C with agitation (600 rpm), protected from the light. Samples were centrifuged again under the same conditions, and finally resuspended in buffer (100 mM phosphate, pH 7.0).

**Dityrosine Cross-Linking by UV Irradiation.** NY7, QY7, and SY7 peptide fibrils were centrifuged at 12 000g for 30 min. Pelleted fibrils were resuspended in buffer (100 mM phosphate, pH 7.0). Spectra and DiY cross-link kinetics were acquired at 25 °C under agitation (600 rpm). Tyrosine spectra were recorded exciting at 274 nm and recording in the 285–500 nm range using a bandwidth of 5 nm on a Jasco FP-8200 fluorescence spectrophotometer (Jasco Corporation, Japan). DiY cross-linking was induced by exposing the sample to an excitation wavelength of 280 nm with a bandwidth of 20 nm. DiY formation was followed by monitoring fluorescence at 410 nm with a bandwidth of 5 nm. UV irradiation was stopped when a fluorescence intensity plateau was reached to avoid excessive photobleaching. DiY formation kinetics were fitted to a one-step reaction using GraphPad Prism 5 (GraphPad Software, USA).

**Dityrosine Cross-Linking by Cu<sup>2+</sup>-Catalyzed Oxidation.** SY7 peptide fibrils were obtained as described and centrifuged at 12 000g for 30 min. Pelleted fibrils were resuspended in buffer (100 mM phosphate, pH 7.0), and 50 μM Cu<sup>2+</sup> were added to the reaction. To start the oxidation reaction, 1.25 mM H<sub>2</sub>O<sub>2</sub> was added, and sample was incubated at 37 °C with agitation (400 rpm) for 24 h. To stop the reaction, 1.25 mM EDTA was added. Control reactions were performed by incubating peptide alone with 50 mM Cu<sup>2+</sup> and with 1.25 mM H<sub>2</sub>O<sub>2</sub> under the same conditions. DiY was assessed measuring tyrosine fluorescent spectra in a Jasco FP-8200 fluorescence spectrophotometer (Jasco Corporation, Japan) with an excitation for tyrosine of 274 nm and recording spectra in the 285–500 nm range, with an excitation for DiY of 320 nm, and recording spectra in the 350–500 nm range, with an excitation and emission bandwidth of 5 nm.

**Denaturation of Cross-Linked and Non-Cross-Linked Self-Assembled Peptide Fibrils with Denaturant Agents.** NY7, QY7, and SY7 fibrils were obtained as described previously in a 1 mL final volume and cross-linked using the previously described methods including non-cross-linked controls. Then, 500 μL of each reaction was mixed with 25 μM Th-T and 4 M guanidinium thiocyanate (GTC) for NY7 and SY7; 6 M GTC for QY7 in a quartz cuvette (1 mL final volume) and incubated for 2000 s at 25 °C under agitation (600 rpm) in the fluorescence spectrophotometer. Th-T fluorescence

was recorded with a data pitch of 1 s using an excitation wavelength of 445 nm, recording at 485 nm with an excitation and emission bandwidth of 5 nm. Denaturing curves were fitted to a one-step reaction using GraphPad Prism 5 (GraphPad Software, USA).

**Chemical Denaturation of Hexapeptides and Heptapeptides Fibrils with GTC.** First, 500 μL of 200 μM NY6, NY7, QY6, QY7, SY6, and SY7 fibrils were mixed with 25 μM Th-T and 4 or 6 M guanidinium thiocyanate (GTC) in a quartz cuvette (1 mL final volume) and incubated for 2000 s at 25 °C under agitation (600 rpm). Th-T fluorescence was recorded with a data pitch of 1 s using an excitation wavelength of 445 nm and recorded at 485 nm with an excitation and emission bandwidth of 5 nm. Denaturing curves were fitted to a one-step reaction using GraphPad Prism 5 (GraphPad Software, USA).

**Electropolymerization of Pyrrole with Peptides.** Pyrrole and L-tyrosine were purchased from Sigma-Aldrich. Sodium chloride was obtained from Panreac. Copper(II) chloride was purchased from Acros Organics. The electropolymerization of pyrrole has been done by chronoamperometry in NaCl 0.1 M using a lab-made three-electrode cell, with a platinum wire as counter electrode, a silver wire as a reference electrode, and an indium tin oxide (ITO) electrode as a working electrode. The potential applied to do the electropolymerization was 0.7 V vs Ag/AgCl. The concentration of pyrrole in the solution was 50 mM and the concentration of the different peptides was 250 μM. The total volume used was 1 mL. The sunken area of ITO electrode was 0.7 × 0.8 cm<sup>2</sup>.

**Chemical Polymerization of Pyrrole with Peptides.** The chemical polymerization of pyrrole was done by mixing the different peptides (NY7, QY7, and SY7) with a 4 mM copper(II) chloride solution and then exposing it to distilled pyrrole vapor. As a reference, a solution of plain CuCl<sub>2</sub> with L-tyrosine was exposed to distilled pyrrole vapor.

## ASSOCIATED CONTENT

### S Supporting Information

The Supporting Information is available free of charge on the ACS Publications website at DOI: 10.1021/acsnano.8b00417.

Biophysical characterization of NY7, QY7, SY7, and GY7 peptides in different buffers and concentrations; TEM micrographs of heptapeptides fibrils at high magnification; cell viability assay to assess heptapeptides fibrils toxicity; TEM images of heptapeptide fibrillar meshes; DiY spectra, DiY formation kinetics, and TEM images; SY7 fibrils DiY formation upon UV-irradiation; disaggregation kinetics in the presence of several denaturing agents; PPy formation by NY7, QY7, and SY7 fibrils and TEM images; biophysical characterization of NY6, QY6, and SY6 peptides; disaggregation kinetics comparing hexapeptides with heptapeptides; IR contributions for NY7, QY7, SY7, and GY7 peptides; lengths and widths of the self-assembled NY7, QY7, SY7, and GY7 fibrils; interplanar distances calculated from the electron diffraction pattern of silver-nanoparticles-conjugated NY7, QY7, and SY7 fibrils (PDF)

## AUTHOR INFORMATION

### Corresponding Author

\*E-mail: salvador.ventura@uab.es.

### ORCID

Marta Díaz-Caballero: 0000-0001-9032-9819

Susanna Navarro: 0000-0001-8160-9536

Isabel Fuentes: 0000-0003-1051-127X

Francesc Teixidor: 0000-0002-3010-2417

Salvador Ventura: 0000-0002-9652-6351

**Notes**

The authors declare no competing financial interest.

**ACKNOWLEDGMENTS**

This work was funded by the Spanish Ministry of Economy and Competitiveness (BFU2013-44763-P and BIO2016-78310-R to S.V.) and ICREA (ICREA-Academia 2015 to S.V.). M. D.-C. was supported by the Spanish Ministry of Science and Innovation via a doctoral grant (FPU14/05786).

**REFERENCES**

- (1) Prusiner, S. B. Molecular Biology of Prion Diseases. *Science* **1991**, *252*, 1515–1522.
- (2) Si, K. Prions: What Are They Good For? *Annu. Rev. Cell Dev. Biol.* **2015**, *31*, 149–169.
- (3) Batlle, C.; Iglesias, V.; Navarro, S.; Ventura, S. Prion-Like Proteins and Their Computational Identification in Proteomes. *Expert Rev. Proteomics* **2017**, *14*, 335–350.
- (4) Chien, P.; Weissman, J. S.; DePace, A. H. Emerging Principles of Conformation-Based Prion Inheritance. *Annu. Rev. Biochem.* **2004**, *73*, 617–656.
- (5) Uptain, S. M.; Lindquist, S. Prions as Protein-Based Genetic Elements. *Annu. Rev. Microbiol.* **2002**, *56*, 703–741.
- (6) Alberti, S.; Halfmann, R.; King, O.; Kapila, A.; Lindquist, S. A Systematic Survey Identifies Prions and Illuminates Sequence Features of Prionogenic Proteins. *Cell* **2009**, *137*, 146–158.
- (7) Espinosa Angarica, V.; Ventura, S.; Sancho, J. Discovering Putative Prion Sequences in Complete Proteomes Using Probabilistic Representations of Q/N-Rich Domains. *BMC Genomics* **2013**, *14*, 316.
- (8) Shahnewaz, M.; Park, K. W.; Mukherjee, A.; Diaz-Espinoza, R.; Soto, C. Prion-Like Characteristics of the Bacterial Protein Microcin E492. *Sci. Rep.* **2017**, *7*, 45720.
- (9) Pallares, I.; Ventura, S. The Transcription Terminator Rho: A First Bacterial Prion. *Trends Microbiol.* **2017**, *25*, 434–437.
- (10) Riek, R.; Eisenberg, D. S. The Activities of Amyloids from a Structural Perspective. *Nature* **2016**, *539*, 227–235.
- (11) Wei, G.; Su, Z.; Reynolds, N. P.; Arosio, P.; Hamley, I. W.; Gazit, E.; Mezzenga, R. Self-Assembling Peptide and Protein Amyloids: From Structure to Tailored Function in Nanotechnology. *Chem. Soc. Rev.* **2017**, *46*, 4661–4708.
- (12) Knowles, T. P.; Buehler, M. J. Nanomechanics of Functional and Pathological Amyloid Materials. *Nat. Nanotechnol.* **2011**, *6*, 469–479.
- (13) Knowles, T. P.; Mezzenga, R. Amyloid Fibrils as Building Blocks for Natural and Artificial Functional Materials. *Adv. Mater.* **2016**, *28*, 6546–6561.
- (14) Zhou, X. M.; Entwistle, A.; Zhang, H.; Jackson, A. P.; Mason, T. O.; Shimanovich, U.; Knowles, T. P.; Smith, A. T.; Sawyer, E. B.; Perrett, S. Self-Assembly of Amyloid Fibrils That Display Active Enzymes. *ChemCatChem* **2014**, *6*, 1961–1968.
- (15) An, B.; Wang, X.; Cui, M.; Gui, X.; Mao, X.; Liu, Y.; Li, K.; Chu, C.; Pu, J.; Ren, S.; Wang, Y.; et al. Diverse Supramolecular Nanofiber Networks Assembled by Functional Low-Complexity Domains. *ACS Nano* **2017**, *11*, 6985–6995.
- (16) Scheibel, T.; Parthasarathy, R.; Sawicki, G.; Lin, X. M.; Jaeger, H.; Lindquist, S. L. Conducting Nanowires Built by Controlled Self-Assembly of Amyloid Fibers and Selective Metal Deposition. *Proc. Natl. Acad. Sci. U. S. A.* **2003**, *100*, 4527–4532.
- (17) Zhou, X. M.; Shimanovich, U.; Herling, T. W.; Wu, S.; Dobson, C. M.; Knowles, T. P.; Perrett, S. Enzymatically Active Microgels from Self-Assembling Protein Nanofibrils for Microflow Chemistry. *ACS Nano* **2015**, *9*, 5772–5781.
- (18) Men, D.; Zhang, Z. P.; Guo, Y. C.; Zhu, D. H.; Bi, L. J.; Deng, J. Y.; Cui, Z. Q.; Wei, H. P.; Zhang, X. E. An Auto-Biotinylated Bifunctional Protein Nanowire for Ultra-Sensitive Molecular Biosensing. *Biosens. Bioelectron.* **2010**, *26*, 1137–1141.
- (19) Arora, A.; Ha, C.; Park, C. B. Insulin Amyloid Fibrillation at above 100 Degrees C: New Insights into Protein Folding under Extreme Temperatures. *Protein Sci.* **2004**, *13*, 2429–2436.
- (20) Buell, A. K.; Dhulesia, A.; Mossuto, M. F.; Cremades, N.; Kumita, J. R.; Dumoulin, M.; Welland, M. E.; Knowles, T. P. J.; Salvatella, X.; Dobson, C. M. Population of Nonnative States of Lysozyme Variants Drives Amyloid Fibril Formation. *J. Am. Chem. Soc.* **2011**, *133*, 7737–7743.
- (21) Pastor, M. T.; Esteras-Chopo, A.; Serrano, L. Hacking the Code of Amyloid Formation: The Amyloid Stretch Hypothesis. *Prion* **2007**, *1*, 9–14.
- (22) Ventura, S.; Zurdo, J.; Narayanan, S.; Parreno, M.; Mangues, R.; Reif, B.; Chiti, F.; Giannoni, E.; Dobson, C. M.; Aviles, F. X.; et al. Short Amino Acid Stretches Can Mediate Amyloid Formation in Globular Proteins: The Src Homology 3 (SH3) Case. *Proc. Natl. Acad. Sci. U. S. A.* **2004**, *101*, 7258–7263.
- (23) Sabate, R.; Rousseau, F.; Schymkowitz, J.; Batlle, C.; Ventura, S. Amyloids or Prions? That Is the Question. *Prion* **2015**, *9*, 200–206.
- (24) Toombs, J. A.; Petri, M.; Paul, K. R.; Kan, G. Y.; Ben-Hur, A.; Ross, E. D. De Novo Design of Synthetic Prion Domains. *Proc. Natl. Acad. Sci. U. S. A.* **2012**, *109*, 6519–6524.
- (25) Ross, E. D.; Edskes, H. K.; Terry, M. J.; Wickner, R. B. Primary Sequence Independence for Prion Formation. *Proc. Natl. Acad. Sci. U. S. A.* **2005**, *102*, 12825–12830.
- (26) Toombs, J. A.; McCarty, B. R.; Ross, E. D. Compositional Determinants of Prion Formation in Yeast. *Mol. Cell. Biol.* **2010**, *30*, 319–332.
- (27) Kwon, I.; Kato, M.; Xiang, S.; Wu, L.; Theodoropoulos, P.; Mirzaei, H.; Han, T.; Xie, S.; Corden, J. L.; McKnight, S. L. Phosphorylation-Regulated Binding of RNA Polymerase II to Fibrous Polymers of Low-Complexity Domains. *Cell* **2013**, *155*, 1049–1060.
- (28) Schwartz, J. C.; Wang, X.; Podell, E. R.; Cech, T. R. RNA Seeds Higher-Order Assembly of FUS Protein. *Cell Rep.* **2013**, *5*, 918–925.
- (29) Pak, C. W.; Kosno, M.; Holehouse, A. S.; Padrick, S. B.; Mittal, A.; Ali, R.; Yunus, A. A.; Liu, D. R.; Pappu, R. V.; Rosen, M. K. Sequence Determinants of Intracellular Phase Separation by Complex Coacervation of a Disordered Protein. *Mol. Cell* **2016**, *63*, 72–85.
- (30) Kato, M.; Han, T. W.; Xie, S.; Shi, K.; Du, X.; Wu, L. C.; Mirzaei, H.; Goldsmith, E. J.; Longgood, J.; Pei, J.; et al. Cell-Free Formation of RNA Granules: Low Complexity Sequence Domains Form Dynamic Fibers within Hydrogels. *Cell* **2012**, *149*, 753–767.
- (31) Harper, J. D.; Wong, S. S.; Lieber, C. M.; Lansbury, P. T. Observation of Metastable Abeta Amyloid Protofibrils by Atomic Force Microscopy. *Chem. Biol.* **1997**, *4*, 119–125.
- (32) Sunde, M.; Blake, C. The Structure of Amyloid Fibrils by Electron Microscopy and X-Ray Diffraction. *Adv. Protein Chem.* **1997**, *50*, 123–159.
- (33) Nelson, R.; Sawaya, M. R.; Balbirnie, M.; Madsen, A. O.; Riek, C.; Grothe, R.; Eisenberg, D. Structure of the Cross-Beta Spine of Amyloid-Like Fibrils. *Nature* **2005**, *435*, 773–778.
- (34) Walsh, I.; Seno, F.; Tosatto, S. C.; Trovato, A. PASTA 2.0: An Improved Server for Protein Aggregation Prediction. *Nucleic Acids Res.* **2014**, *42* (W1), W301–W307.
- (35) Fernandez-Escamilla, A. M.; Rousseau, F.; Schymkowitz, J.; Serrano, L. Prediction of Sequence-Dependent and Mutational Effects on the Aggregation of Peptides and Proteins. *Nat. Biotechnol.* **2004**, *22*, 1302–1306.
- (36) Raz, Y.; Rubinov, B.; Matmor, M.; Rapaport, H.; Ashkenasy, G.; Miller, Y. Effects of Mutations in De Novo Designed Synthetic Amphiphilic Beta-Sheet Peptides on Self-Assembly of Fibrils. *Chem. Commun. (Cambridge, U. K.)* **2013**, *49*, 6561–6563.
- (37) Miller, Y.; Ma, B.; Nussinov, R. Polymorphism in Self-Assembly of Peptide-Based Beta-Hairpin Contributes to Network Morphology and Hydrogel Mechanical Rigidity. *J. Phys. Chem. B* **2015**, *119*, 482–490.
- (38) Artimo, P.; Jonnalagedda, M.; Arnold, K.; Baratin, D.; Csardi, G.; de Castro, E.; Duvaud, S.; Fleig, V.; Fortier, A.; Gasteiger, E.; et al. ExPASY: SIB Bioinformatics Resource Portal. *Nucleic Acids Res.* **2012**, *40* (W1), W597–W603.

- (39) Zurdo, J.; Guijarro, J. I.; Jimenez, J. L.; Saibil, H. R.; Dobson, C. M. Dependence on Solution Conditions of Aggregation and Amyloid Formation by an SH3 Domain. *J. Mol. Biol.* **2001**, *311*, 325–340.
- (40) Amaro, M.; Birch, D. J.; Rolinski, O. J. Beta-Amyloid Oligomerisation Monitored by Intrinsic Tyrosine Fluorescence. *Phys. Chem. Chem. Phys.* **2011**, *13* (14), 6434–6441.
- (41) Sabate, R.; Rodriguez-Santiago, L.; Sodupe, M.; Saupe, S. J.; Ventura, S. Thioflavin-T Excimer Formation Upon Interaction with Amyloid Fibers. *Chem. Commun. (Cambridge, U. K.)* **2013**, *49*, 5745–5747.
- (42) Klunk, W. E.; Pettegrew, J. W.; Abraham, D. J. Quantitative Evaluation of Congo Red Binding to Amyloid-Like Proteins with a Beta-Pleated Sheet Conformation. *J. Histochem. Cytochem.* **1989**, *37*, 1273–1281.
- (43) Serpell, L. C. Alzheimer's Amyloid Fibrils: Structure and Assembly. *Biochim. Biophys. Acta, Mol. Basis Dis.* **2000**, *1502*, 16–30.
- (44) Partlow, B. P.; Applegate, M. B.; Omenetto, F. G.; Kaplan, D. L. Dityrosine Cross-Linking in Designing Biomaterials. *ACS Biomater. Sci. Eng.* **2016**, *2*, 2108–2121.
- (45) Ding, Y.; Li, Y.; Qin, M.; Cao, Y.; Wang, W. Photo-Cross-Linking Approach to Engineering Small Tyrosine-Containing Peptide Hydrogels with Enhanced Mechanical Stability. *Langmuir* **2013**, *29*, 13299–13306.
- (46) Min, K.-I.; Lee, S.-W.; Lee, E.-H.; Lee, Y.-S.; Yi, H.; Kim, D.-P. Facile Nondestructive Assembly of Tyrosine-Rich Peptide Nanofibers as a Biological Glue for Multicomponent-Based Nanoelectrode Applications. *Adv. Funct. Mater.* **2018**, *28*, 1705729.
- (47) Xie, J.; Lee, J. Y.; Wang, D. I.; Ting, Y. P. Silver Nanoplates: From Biological to Biomimetic Synthesis. *ACS Nano* **2007**, *1*, 429–439.
- (48) Lee, V. W.-M.; Li, H.; Lau, T. C.; Guevremont, R.; Siu, K. W. M. Relative Silver(I) Ion Binding Energies of Alpha-Amino Acids: A Determination by Means of the Kinetic Method. *J. Am. Soc. Mass Spectrom.* **1998**, *9*, 760–766.
- (49) Jang, H. S.; Lee, J. H.; Park, Y. S.; Kim, Y. O.; Park, J.; Yang, T. Y.; Jin, K.; Lee, J.; Park, S.; You, J. M.; et al. Tyrosine-Mediated Two-Dimensional Peptide Assembly and Its Role as a Bio-Inspired Catalytic Scaffold. *Nat. Commun.* **2014**, *5*, 3665.
- (50) Asavapiriyant, S.; Chandler, G. K.; Gunawardena, G. A.; Pletcher, D. The Electrodeposition of Polypyrrole Films from Aqueous Solutions. *J. Electroanal. Chem. Interfacial Electrochem.* **1984**, *177*, 229–244.
- (51) Luo, F.; Gui, X.; Zhou, H.; Gu, J.; Li, Y.; Liu, X.; Zhao, M.; Li, D.; Li, X.; Liu, C. Atomic Structures of FUS LC Domain Segments Reveal Bases for Reversible Amyloid Fibril Formation. *Nat. Struct. Mol. Biol.* **2018**, *25*, 341–346.
- (52) Burke, K. A.; Janke, A. M.; Rhine, C. L.; Fawzi, N. L. Residue-by-Residue View of *in Vitro* Fus Granules That Bind the C-Terminal Domain of RNA Polymerase II. *Mol. Cell* **2015**, *60*, 231–241.
- (53) Molliex, A.; Temirov, J.; Lee, J.; Coughlin, M.; Kanagaraj, A. P.; Kim, H. J.; Mittag, T.; Taylor, J. P. Phase Separation by Low Complexity Domains Promotes Stress Granule Assembly and Drives Pathological Fibrillization. *Cell* **2015**, *163*, 123–133.
- (54) Han, T. W.; Kato, M.; Xie, S.; Wu, L. C.; Mirzaei, H.; Pei, J.; Chen, M.; Xie, Y.; Allen, J.; Xiao, G.; et al. Cell-Free Formation of RNA Granules: Bound RNAs Identify Features and Components of Cellular Assemblies. *Cell* **2012**, *149*, 768–779.
- (55) Lin, Y.; Protter, D. S.; Rosen, M. K.; Parker, R. Formation and Maturation of Phase-Separated Liquid Droplets by RNA-Binding Proteins. *Mol. Mol. Cell* **2015**, *60*, 208–219.
- (56) Patel, A.; Lee, H. O.; Jawerth, L.; Maharana, S.; Jahnel, M.; Hein, M. Y.; Stoynov, S.; Mahamid, J.; Saha, S.; Franzmann, T. M.; et al. A Liquid-to-Solid Phase Transition of the Als Protein Fus Accelerated by Disease Mutation. *Cell* **2015**, *162*, 1066–1077.
- (57) Cuesta, I. G.; Sanchez de Meras, A. M. Energy Interactions in Amyloid-Like Fibrils from NNQQQNY. *Phys. Chem. Chem. Phys.* **2014**, *16*, 4369–4377.
- (58) Gazit, E. A Possible Role for Pi-Stacking in the Self-Assembly of Amyloid Fibrils. *FASEB J.* **2002**, *16*, 77–83.
- (59) Reches, M.; Gazit, E. Casting Metal Nanowires within Discrete Self-Assembled Peptide Nanotubes. *Science* **2003**, *300*, 625–627.
- (60) Gallagher-Jones, M.; Glynn, C.; Boyer, D. R.; Martynowycz, M. W.; Hernandez, E.; Miao, J.; Zee, C.; Novikova, I. V.; Goldschmidt, L.; McFarlane, H. T. Sub-Ångström Cryo-Em Structure of a Prion Protofibril Reveals a Polar Clasp. *Nat. Struct. Mol. Biol.* **2018**, *25*, 131.
- (61) Clements, K. A.; Acevedo-Jake, A. M.; Walker, D. R.; Hartgerink, J. D. Glycine Substitutions in Collagen Heterotrimers Alter Triple Helical Assembly. *Biomacromolecules* **2017**, *18*, 617–624.
- (62) Fukushima, Y. Genetically Engineered Syntheses of Tandem Repetitive Polypeptides Consisting of Glycine-Rich Sequence of Spider Dragline Silk. *Biopolymers* **1998**, *45*, 269–279.
- (63) Giasson, B. I.; Murray, I. V.; Trojanowski, J. Q.; Lee, V. M. A Hydrophobic Stretch of 12 Amino Acid Residues in the Middle of Alpha-Synuclein Is Essential for Filament Assembly. *J. Biol. Chem.* **2001**, *276*, 2380–2386.
- (64) de Groot, N. S.; Aviles, F. X.; Vendrell, J.; Ventura, S. Mutagenesis of the Central Hydrophobic Cluster in Abeta42 Alzheimer's Peptide. Side-Chain Properties Correlate with Aggregation Propensities. *FEBS J.* **2006**, *273*, 658–668.